March 26, 2025
Typeset using LaTeX **default** style in AASTeX7

The Schwarzschild Solution and it's role in the Advance of the Perihelion of Mercury

219046104[1]
Department of Physics and Astronomy

[1] *University of Leicester*

ABSTRACT

This report presents a comprehensive investigation of the Schwarzschild solution and its implications for both free-fall trajectories and the advance of Mercury's perihelion, while also discussing extensions to more general spacetimes. The Schwarzschild metric, representing a static, spherically symmetric vacuum solution to Einstein's field equations, is examined in detail, highlighting its physical interpretation, inherent coordinate singularities, and its asymptotically flat nature. By deriving the geodesic equations, we demonstrate that a test particle falling radially into a Schwarzschild black hole experiences a finite proper time to cross the event horizon, even though an external observer perceives an infinite coordinate time—a phenomenon clearly illustrated through Penrose diagrams and the maximal Kruskal–Szekeres extension. Furthermore, the report derives the relativistic correction to Newtonian orbital dynamics that leads to the perihelion precession of Mercury, showing that the extra curvature-induced term in the orbital equation causes the orbit to precess by an amount proportional to $3GM^2/(c^2h^2)$. Extensions to the Reissner–Nordström and Kerr spacetimes are also discussed, where additional factors such as electric charge and rotation modify the effective gravitational potential and orbital dynamics, respectively. Despite the robustness of these analytical methods, the report also addresses their limitations, including the test particle assumption, the perturbative treatment of relativistic corrections, and the reliance on high degrees of symmetry.

1. INTRODUCTION

General relativity is a revolutionary theory of gravity developed by Albert Einstein that fundamentally redefines how we perceive the interaction between matter, energy, and the fabric of the universe. In this framework, gravity is not considered a force in the traditional sense but rather an effect of the curvature of spacetime, a four-dimensional continuum that fuses the three dimensions of space with time. According to the theory, the presence of mass and energy causes spacetime to curve, and this curvature in turn influences the motion of objects. For instance, a planet orbiting a star is simply following a path determined by the distorted geometry of spacetime around the star.

1.1. *Einstein Field Equations*

Einstein's general theory of relativity describes the gravitational field by means of a symmetric metric tensor $g_{\mu\nu}$ defined on a four-dimensional pseudo-Riemannian manifold (A. A. Shaikh et al. 2023). The gravitational interaction is not treated as a force in the traditional sense; instead, it is interpreted as the manifestation of spacetime curvature. The fundamental equations governing this curvature are the Einstein field equations, which consist of 10 coupled, nonlinear partial differential equations in four spacetime coordinates (S. M. Carroll 2019). They are given by

$$G_{\mu\nu} \equiv R_{\mu\nu} - \frac{1}{2} g_{\mu\nu} R = \kappa\, T_{\mu\nu}, \tag{1}$$

where:

- $G_{\mu\nu}$ is the Einstein tensor, encoding the curvature of spacetime;
- $R_{\mu\nu}$ is the Ricci curvature tensor;

- R is the Ricci scalar, i.e. the trace of the Ricci tensor;
- $g_{\mu\nu}$ is the metric tensor;
- $T_{\mu\nu}$ is the stress–energy tensor representing the distribution of matter and energy;
- $\kappa = \frac{8\pi G}{c^4}$ is the coupling constant, with G as Newton's gravitational constant and c the speed of light.

Due to their nonlinear nature, these equations cannot, in general, be solved exactly in closed form. In many instances, they are reformulated as self-coupled integral equations (D. W. SCIAMA et al. 1969), and analytic or numerical approximation methods are employed to study specific physical scenarios.

"Exact solutions" in general relativity are not uniquely defined. In many cases, an exact solution is one in which all the metric functions are expressed explicitly in terms of elementary functions or well-known special functions (M. A. MacCallum 2013). However, the term is sometimes used more broadly to include solutions that are defined only up to the solution of additional differential equations. Typically, such solutions are obtained by imposing additional symmetries, such as spherical symmetry, or prescribing a special form for the curvature tensor (M. A. MacCallum 2013). It is also important to note that an exact solution does not inherently have a unique physical interpretation. For example, the Schwarzschild solution, an exact vacuum solution, can represent either the exterior gravitational field of a static, spherically symmetric mass or, under different circumstances, the interaction region following the collision of two plane gravitational waves. Furthermore, distinct physical sources may sometimes produce the same exact metric.

The Einstein field equations can be derived from a variational principle. Specifically, one begins with the Einstein–Hilbert action (D. Tong 2019)

$$S = \frac{1}{2\kappa} \int R\sqrt{-g}\, d^4x + S_{\text{matter}},$$

where the gravitational Lagrangian density is

$$\mathcal{L} = \frac{1}{2\kappa} R\sqrt{-g}.$$

By requiring that the action S is stationary with respect to variations of the metric $g_{\mu\nu}$, one obtains the Euler–Lagrange equations for the gravitational field. These equations are exactly the Einstein field equations given above.//

2. THE FIRST NON-TRIVIAL SOLUTION: SCHWARZSCHILD SOLUTION

Einstein field equations are known to be highly nonlinear partial differential equations with numerous exact solutions to them (P. G. Bergmann 1962). The simplest of the exact solution is of Schwarzschild. The Schwarzschild line element is given by

$$ds^2 = \left(1 - \frac{2m}{r}\right) dt^2 - \left(1 - \frac{2m}{r}\right)^{-1} dr^2 - r^2(d\theta^2 + sin^2(\theta) d\phi^2) \tag{2}$$

where:

1. m $= \frac{GM}{c^2}$ is the geometric mass
2. r $\rightarrow$ radial coordinate
3. t $\rightarrow$ is the coordinate time (measured by a stationary clock at infinity
4. $\theta \rightarrow$ is the polar angle
5. $\phi \rightarrow$ is the azimuthal angle

Therefore, the metric tensor for this is

$$g_{ab} = \begin{bmatrix} \left(1 - \frac{2GM}{c^2 r}\right) & 0 & 0 & 0 \\ 0 & -\left(1 - \frac{2GM}{c^2 r}\right)^{-1} & 0 & 0 \\ 0 & 0 & -r^2 & 0 \\ 0 & 0 & 0 & -r^2 sin^2(\theta) \end{bmatrix} \tag{3}$$

The given line element can be derived by finding the non-vanishing components of the mixed Einstein tensor. Only a few of these components turn out to be non-zero. Moreover, the contracted Bianchi identities which guarantee the covariant conservation of the energy momentum tensor impose additional constraints (P. Petersen 2011). In particular, these identities reveal that one of the tensor equations is automatically satisfied when the remaining ones vanish. As a result, the full set of Einstein field equations in vacuum (where $T_{\mu\nu} = 0$) reduces to only three independent equations.

2.1. *Stationary solution*

In simple terms, a solution is said to be stationary if it is time-independent. This does not mean that the solution is in no way evolutionary, but simply time does not enter into it explicitly (R. D'Inverno 1992).
This can be explained better using something called Killing vectors. Killing vector, after Wilhelm Killing, is a vector field $\mathbf{X}$ that preserves the metric tensor. In layback manner, if you move the metric g a little bit by $\mathbf{X}$ and g doesn't change, then $\mathbf{X}$ is a Killing vector. This invariance is mathematically expressed by the vanishing of the Lie derivative of the metric with respect to $\mathbf{X}$:

$$\mathscr{L}_X g_{ab} = 0 \tag{4}$$

In other words, the Lie derivative measures the change in the metric when it is dragged along the vector field $\mathbf{X}$. If the Lie derivative is zero, the metric does not change under the corresponding infinitesimal coordinate transformation, indicating that the spacetime geometry is invariant under the flow generated by $\mathbf{X}$ (J. L. Friedman & N. Stergioulas 2013).

A metric will also be stationary if there exists a special coordinate system in which the metric is visibly time-independent, i.e.

$$\frac{\partial g_{ab}}{\partial x^0} \overset{*}{=} 0 \tag{5}$$

In a general coordinate system, the metric components may explicitly depend on all coordinates, so the condition expressed in equation 5 must be formulated in a coordinate-invariant way. To accomplish this, we introduce a vector field (R. D'Inverno 1992)

$$X^a = \delta^a_0 \tag{6}$$

then,

$$\mathscr{L}_X g_{ab} = X^c g_{abc} + g_{ac} X^c, b + g_{bc} X^c, a = \delta^c_0 g_{ab,c} = 0 \tag{7}$$

$\mathscr{L}_X g_{ab}$ is a tensor, which means that if it vanishes in one coordinate system, it must vanish in all coordinate systems. In an adapted coordinate system where $\partial_b X^c = 0$ and $\partial_a X^c = 0$, this condition implies that $\mathbf{X^a}$ is a Killing vector vector field. Conversely, if we have a timelike Killing vector field $\mathbf{X^a}$, one can always choose a coordinate system that is adapted to i.e. (R. D'Inverno 1992)

$$\mathscr{L}_x g_{ab} = 0 \tag{8}$$

Therefore, a space-time is said to be stationary if and only if it admits a timelike Killing vector field.

2.2. *Static solution*

If a solution is stationary, then in a coordinate system adapted to the symmetry the metric is independent of time, yet the line element may still contain mixed terms of the form $dx^0 dx^\nu$ (R. D'Inverno 1992). In contrast, for a static metric we expect these cross terms to vanish. To illustrate, consider the interval between two events with coordinates (x^0, x^1, x^2, x^3) and $(x^0 + dx^0, x^1 + dx^1, x^2, x^3)$ in this special coordinate system. The corresponding line element is:

$$ds^2 = g_{00}(dx^0)^2 + 2g_{01}dx^0 dx^1 + g_{11}(dx^1)^2 \tag{9}$$

where all the metric tensor elements depend on x^ν only. Under a time reversal

$$x^0 \longrightarrow x'^0 = -x^0 \tag{10}$$

then, the only term that changes in the line element is

$$g_{01}dx^0 dx^1 \longrightarrow -g_{01}dx^0 dx^1 \tag{11}$$

With the other terms unaffected by the coordinate transformation, and given that the line element is invariant under any coordinate transformation, the only way for it to remain unchanged under a time-reversal transformation is if the mixed term g_{01} vanishes. By a similar argument, g_{02} and g_{03} must vanish. Therefore, in this special coordinate system there are no cross terms in the line element (R. D'Inverno 1992).

Thus, in a static spacetime there exists a coordinate system adapted to the timelike Killing vector field in which the metric is time-independent and the line element contains no mixed time-space terms (i.e., $g_{0\nu} = 0$) (R. D'Inverno 1992).

Having clarified the differences between static and stationary spacetimes, we are now in a position to analyse the **Schwarzschild solution** in detail and explore its distinctive geometric and physical properties.

2.3. *Time-independence and Stationarity*

If we restrict attention to the exterior region, i.e. $r > 2m$, where the coordinates t and r are timelike and spacelike respectively, it is immediate from the Schwarzschild line element that

$$\frac{\partial g_{ab}}{\partial t} = 0 \quad \text{for all } a \text{ and } b.$$

A spacetime whose metric components are time-independent is said to be stationary. Moreover, in Schwarzschild coordinates the metric does not depend on the time coordinate t; therefore, the natural choice for the Killing vector field is:

$$X^a = \delta^a_0, \tag{12}$$

in which the coordinates have components $X^0 = \delta^0_0 = 1$ and $X^i = \delta^i_0 = 0$ (for $i = 1, 2, 3$ corresponding to r, θ, ϕ). Since the metric components are time-independent, the Lie derivative is

$$\mathscr{L}_X g_{ab} = 0, \tag{13}$$

proving again that the solution is stationary (R. D'Inverno 1992).

2.4. *Hypersurface-Orthogonality and Staticity*

A stationary spacetime is called static if, in addition to being time-independent, the timelike Killing vector field is hypersurface-orthogonal. This means that there exists a family of spacelike hypersurfaces (i.e., surfaces of constant time) to which the Killing vector is everywhere orthogonal (H. Weyl 2010–2011). One way to verify this property is to compute the covector X_a associated with the Killing vector X^a:

$$X_a = g_{ab}X^b = g_{ab}\delta^b_0 = g_{0a}. \tag{14}$$

For the Schwarzschild metric, we have:

$$X^a = (g_{00}, g_{01}, g_{02}, g_{03}) = \left(1 - \frac{2m}{r},\, 0,\, 0,\, 0\right). \tag{15}$$

Thus, X^a is hypersurface-orthogonal, which can be expressed in the form

$$X_a = \lambda\, f_{,a},$$

where we choose $f(x^a) = t$ (so that $f_{,0} = \partial_0 t = \delta^0_0$) and $\lambda = X^2 = g_{00}$. Since the Killing field X^a is proportional to the gradient of the scalar function t, it follows by Frobenius' theorem (B. A. Sherwood 2011) that X^a is hypersurface-orthogonal, and hence the solution is static. Alternatively, one observes from the line element that the metric is invariant under the reflection $t \longrightarrow -t$ and under time translations ($t \longrightarrow t + \text{constant}$), further confirming the staticity of the solution (H. Weyl 2010–2011). We have thus proved the following somewhat unexpected result:

Birkhoff's Theorem: Any spherically symmetric solution of Einstein's vacuum field equations must be static (and asymptotically flat). This means that even if one were to consider a spherically symmetric gravitational field

that might, in principle, be time-dependent, the field equations force the solution to be independent of time (W. Van Oosterhout 2019).

This result is surprising because, in Newtonian gravity, spherical symmetry does not impose any restrictions on time dependence. This contrast underscores the unique nature of the strong non-linearity inherent in the Einstein field equations and the range of solutions they permit.

If a spherically symmetric source is restricted to the region r $\leq$ a for some r $\geq$ 2m, then the solution for r $>$ a must be the Schwarzschild exterior solution. However, the converse is not true: a source which gives rise to an exterior Schwarzschild solution is not necessarily spherically symmetric.

Furthermore, if we take the limit of the Schwarzschild line element as r$\longrightarrow\infty$, then we obtain the flat space metric (Minkowski space-time) in spherical polar coordinates:

$$ds^2 = dt^2 - dr^2 - r^2(d\theta^2 + sin^2\theta d\phi^2) \tag{16}$$

We have therefore shown that a spherically symmetric solution, in this case Schwarzschild solution is necessarily asymptotically flat.

Hence the **Schwarzschild solution** is a spherically symmetric, static, vacuum (i.e. $T_{\mu\nu}$) solution.

2.5. *Limitations of the Schwarzschild Solution*

The Schwarzschild solution is derived by solving the Einstein field equations under the condition that the stress-energy tensor $T_{\mu\nu} = 0$; that is, it describes a vacuum. In practice, it accurately describes the spacetime outside a spherically symmetric, non-rotating mass. To describe the interior of a star or any matter distribution, one must match the Schwarzschild exterior to an appropriate interior solution (like the interior Schwarzschild solution).

In Schwarzschild coordinates, it is clear that if we take r = 2m $\left(\frac{2GM}{c^2}, \text{the Schwarzschild radius}\right)$, the metric is not valid and appears to be singular. However, this is a coordinate singularity-the true spacetime is regular there. Similarly, taking r = 0, the Schwarzschild solution has a genuine curvature singularity where tidal forces diverge, signalling that the classical theory of general relativity breaks down. This "singularity" is not just a coordinate problem but a location where spacetime itself is no longer well-defined. Clearly, then, the Schwarzschild coordinate system is inappropriate for describing this motion.

The Schwarzschild solution also assumes that the source is perfectly symmetric unchanging in time (static). This precludes its application to objects with rotation or any time-dependent (dynamic) behavior. For rotating bodies or charged objects, other solutions such as the Kerr (for rotation) or Reissner–Nordström (for charge) metrics are needed.

2.6. *Causal structure of the Schwarzschild solution*

One way to gain insight into the geometry of the Schwarzschild solution is by examining its causal structure as defined by the light cones. In particular, the Schwarzschild solution, originally defined for

$$2m < r < \infty,$$

can be extended either into the advanced (ingoing) Eddington–Finkelstein coordinates or into the retarded (outgoing) Eddington–Finkelstein coordinates, thereby covering the full range (S. M. Carroll 1997)

$$0 < r < \infty.$$

In contrast, Minkowski spacetime is a geodesically complete manifold. The standard Schwarzschild solution, however, is defined only for $r > r_s$, where

$$r_s = \frac{2GM}{c^2}.$$

At $r = r_s$, one of the metric components becomes singular, which is merely a coordinate singularity rather than a true physical singularity. Consequently, the Schwarzschild coordinates describe only a portion of the entire spacetime (S. M. Carroll 1997).

Similarly, by switching to either the advanced (ingoing) or retarded (outgoing) Eddington-Finkelstein coordinates, the coordinate singularity at r = $\frac{2GM}{c^2}$ can be removed. For example, the ingoing Eddington-Finkelstein metric is (P. Koiran 2021)

$$ds^2 = \left(1 - \frac{2GM}{c^2 r}\right) dv - 2dvdr - r^2(d\theta^2 - sin^2\theta d\phi^2) \tag{17}$$

where v = t + r^* and r^* is the tortoise coordinate. This coordinate system extends smoothly across the event horizon into the black hole interior. However, it covers only one time orientation (in this case, only ingoing null geodesics) and does not include the full structure of the maximally extended Schwarzschild solution (for example it leaves out the "white hole" region and second asymptotically flat region).

To fully understand the causal structure of the Schwarzschild spacetime, one must go beyond the limited patches provided by Schwarzschild and even Eddington–Finkelstein coordinates. Although these coordinate systems successfully describe either the exterior region (Schwarzschild) or smoothly extend through the event horizon in one time direction (Eddington–Finkelstein), as we saw, they do not capture the complete global structure of the spacetime. In contrast, the maximal extension—obtained through a transformation to Kruskal–Szekeres coordinates—reveals additional regions: a second asymptotically flat exterior and a white hole region, in addition to the black hole interior.

A *Penrose-Carter diagram* is constructed by performing a conformal transformation that compactifies the spacetime onto a finite region. This transformation preserves the causal (light-cone) structure—light rays are always at 45°—and allows us to visualize the entire spacetime, including infinity, on a single diagram (B. T. Horizon 2024).

In Penrose diagrams of the maximally extended Schwarzschild spacetime, various regions and boundaries are often labeled with distinct typographic styles to clarify their physical meaning. For example:

- The future null infinity is denoted by $\mathscr{I}^+$ (or sometimes $\mathcal{I}^+$), which represents the asymptotic region where outgoing light rays eventually reach (S. M. Carroll 1997).
- The past null infinity is denoted by $\mathscr{I}^-$ (or $\mathcal{I}^-$), marking the origin of incoming light rays (S. M. Carroll 1997).
- The event horizon is frequently labeled as $\mathcal{H}^+$ (for the future event horizon) and, in the extended diagram, $\mathcal{H}^-$ (for the past event horizon, associated with the white hole region).

These typographic conventions serve two main purposes:

1. They help visually distinguish between regions that have different causal properties. For instance, the use of a script font for $\mathscr{I}$ clearly marks the asymptotic boundary of spacetime, differentiating it from the physical singularity or the horizon.
2. They provide a shorthand that conveys significant information about the role of the boundary or region. For example, by denoting the event horizon with $\mathcal{H}^+$, one immediately understands that this is the surface beyond which events are causally disconnected from the asymptotically flat region.

Such notations are especially useful when discussing the complete causal structure revealed by the Kruskal–Szekeres extension, where the full diagram includes regions corresponding to both a black hole and a white hole, as well as two distinct asymptotically flat regions.

From Schwarzschild to Kruskal–Szekeres Coordinates

The standard Schwarzschild metric is

$$ds^2 = \left(1 - \frac{2M}{r}\right) dt^2 - \frac{dr^2}{1 - \frac{2M}{r}} - r^2 \left(d\theta^2 + \sin^2\theta \, d\phi^2\right). \tag{18}$$

This form is valid only for $r > 2M$ (the exterior) and has a coordinate singularity at the event horizon $r = 2M$.

A maximal extension is achieved by transforming to Kruskal–Szekeres coordinates (T, X). In these coordinates, the metric becomes (J. P. Lemos & D. L. Silva 2021)

$$ds^2 = \frac{32M^3}{r} e^{-r/2M} \left(-dT^2 + dX^2\right) - r^2 \left(d\theta^2 + \sin^2\theta \, d\phi^2\right), \tag{19}$$

with r defined implicitly by

$$T^2 - X^2 = \left(1 - \frac{r}{2M}\right) e^{r/2M}. \tag{20}$$

This metric is regular at the horizon $r = 2M$ and covers additional regions of the spacetime.

Global Structure Revealed by the Penrose Diagram

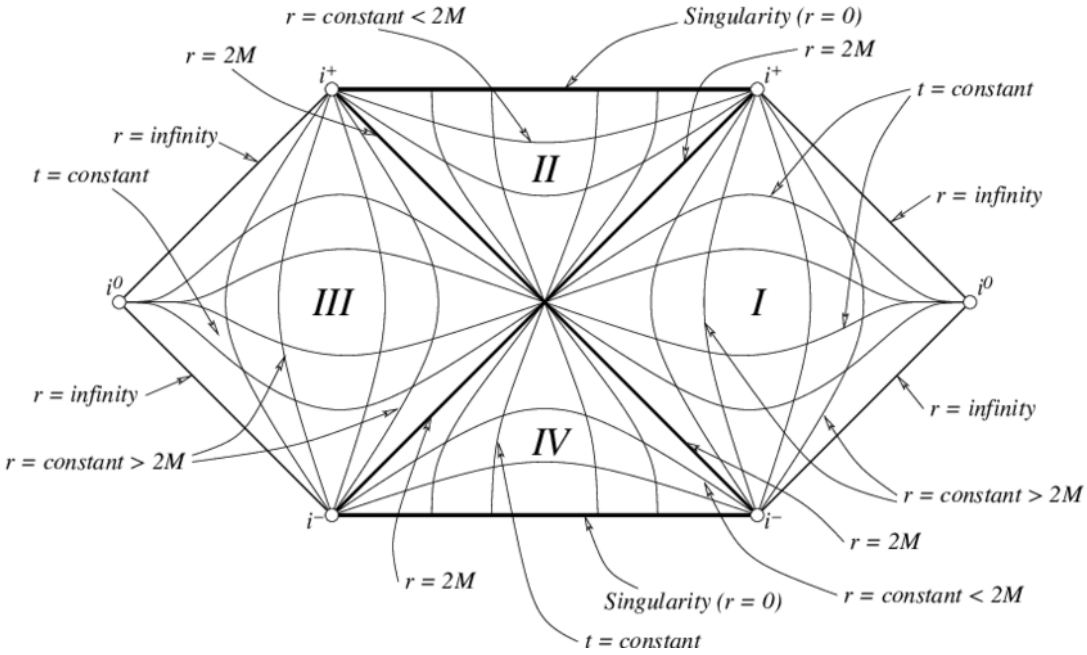

Figure 1. Penrose diagram depicting the causal structure of a Schwarzschild black hole spacetime. The diagram illustrates different regions, labeled I, II, III, and IV, corresponding to various sectors of spacetime around a black hole. Region I represents the exterior of the black hole, while Region II is the interior, where r < 2M with r=0 being the singularity. Region III mirrors Region I and represents another asymptotic universe, and Region IV is the white hole region, a time-reversed version of a black hole. The boundaries at r=2M correspond to the event horizon, while r=0 is the singularity.

The maximally extended Schwarzschild solution contains four regions:

- **Region I:** The right (our) asymptotically flat exterior.
- **Region II:** The black hole interior, where $r < 2M$ and all future-directed timelike curves end at the singularity $r = 0$.
- **Region III:** A second, disconnected asymptotically flat exterior region.
- **Region IV:** The white hole interior (the time-reversal of Region II), from which nothing can enter.

In the Penrose diagram, these regions are mapped onto a compact diagram with finite boundaries. The event horizons are represented by diagonal lines (at 45°) separating the regions. The singularities at $r = 0$ are depicted as horizontal lines, indicating the end of timelike curves. This diagram clearly shows that although an observer in Region I never sees an object cross the event horizon (due to the infinite coordinate time required), the falling object itself experiences only a finite proper time before reaching the singularity (S. M. Carroll 1997; The Center for Cosmology and Particle Physics 2018).

3. FREE FALL INTO BLACK-HOLE

Let us consider a radially infalling free particle. The trajectory for this radially infalling free particle can be calculated by using the fact that for a timelike geodesic, we us proper time τ (time measured by a clock in rest frame relative to the events) as the parameter so that $ds^2 = c^2 d\tau^2$. Let's start with the Schwarzschild line element (in natural units, i.e. G = c = 1)

$$d\tau^2 = \left(1 - \frac{2M}{r}\right) dt^2 - \left(1 - \frac{2M}{r}\right)^{-1} dr^2 - r^2 d\theta^2 - r^2 sin^2\theta d\phi^2 \tag{21}$$

Since our particle is moving solely in a radial direction, we can assume that both θ and ϕ are constants. Therefore the reduced line element is

$$d\tau^2 = \left(1 - \frac{2M}{r}\right) dt^2 - \left(1 - \frac{2M}{r}\right)^{-1} dr^2 \tag{22}$$

The trajectory of the free particle is determined by the geodesic equation which can be derived from the metric. Dividing the equation 22 by $d\tau$ throughout

$$\left(1 - \frac{2M}{r}\right)\left(\frac{dt^2}{d\tau^2}\right) - \left(1 - \frac{2M}{r}\right)^{-1}\left(\frac{dr^2}{d\tau^2}\right) = 1 \tag{23}$$

which can be written as

$$\left(1 - \frac{2M}{r}\right) \dot{t}^2 - \left(1 - \frac{2M}{r}\right)^{-1} \dot{r}^2 = 1 \tag{24}$$

Equation 24 is the normalisation condition for a timelike worldline. This distinguishes timelike geodesics from spacelike geodesics.

Now let's solve for the radial equation of motion. Starting from equation 24 and rearranging it

$$\left(1 - \frac{2M}{r}\right) \dot{t}^2 - 1 = \left(1 - \frac{2M}{r}\right)^{-1} \dot{r}^2 \tag{25}$$

Because the metric is independent of t, there is a conserved quantity (energy per unit mass) associated with the timelike Killing vector ∂_t. The corresponding conjugate momentum is

$$p_t = \frac{\partial \mathcal{L}}{d\dot{t}} = \left(1 - \frac{2M}{r}\right) \dot{t} = k \tag{26}$$

Let equation 26 be equal to k, an arbitrary constant where $k \neq 0$. Therefore, equation 25 can be written as

$$\left(1 - \frac{2M}{r}\right)^{-1} \dot{r}^2 = k\dot{t} - 1 \tag{27}$$

Rearranging for $\dot{r}^2$

$$\dot{r}^{=}(k\dot{t} - 1)\left(1 - \frac{2M}{r}\right) \tag{28}$$

then,

$$\dot{r} = \pm\left[(k\dot{t} - 1)\left(1 - \frac{2M}{r}\right)\right]^{\frac{1}{2}} = \pm\left[k^2 - \left(1 - \frac{2M}{r}\right)\right]^{\frac{1}{2}} \tag{29}$$

Since the particle is falling in, we use the negative root of $\dot{r}$

$$\dot{r} = -\left[k^2 - \left(1 - \frac{2M}{r}\right)\right]^{\frac{1}{2}} \tag{30}$$

Let's take the arbitrary constant k = 1, which corresponds to dropping in a particle with zero initial velocity with respect to the timelike Killing vector at infinity. Then

$$\dot{r} = -\left[1 - \left(1 - \frac{2M}{r}\right)\right]^{\frac{1}{2}} = \left(\frac{2M}{r}\right)^{\frac{1}{2}} \tag{31}$$

Rearranging to keep like terms together

$$\sqrt{r}\frac{dr}{d\tau} = \sqrt{2M} \Longrightarrow \sqrt{r}dr = \sqrt{2M}d\tau \tag{32}$$

Integrating equation 32 both sides

$$\begin{aligned} &\frac{2}{3}r^{\frac{2}{3}} = -\sqrt{2M}\int d\tau \\ \Rightarrow &\frac{2}{3}r^{\frac{2}{3}} = -\sqrt{2M}(\tau + C), (\text{C = constant of integration}) \\ &r = \left(-\frac{3}{2}\sqrt{2M}(\tau + C)\right)^{2/3} \end{aligned} \tag{33}$$

at $\tau = 0$

$$C = \frac{2}{3}\frac{r_0^{3/2}}{\sqrt{2M}} \tag{34}$$

Therefore, the radial equation of motion is

$$r(\tau) = \left(r_0^{3/2} - \frac{3}{2}\sqrt{2M}\tau\right) \tag{35}$$

Using equation 26, we can find the integral for the coordinate time

$$\begin{aligned} &\frac{dt}{d\tau} = \frac{1}{1 - \frac{2M}{r}} \\ &\Rightarrow t(\tau) = \int_0^\tau \frac{d\tau'}{1 - \frac{2M}{r(\tau')}} \end{aligned} \tag{36}$$

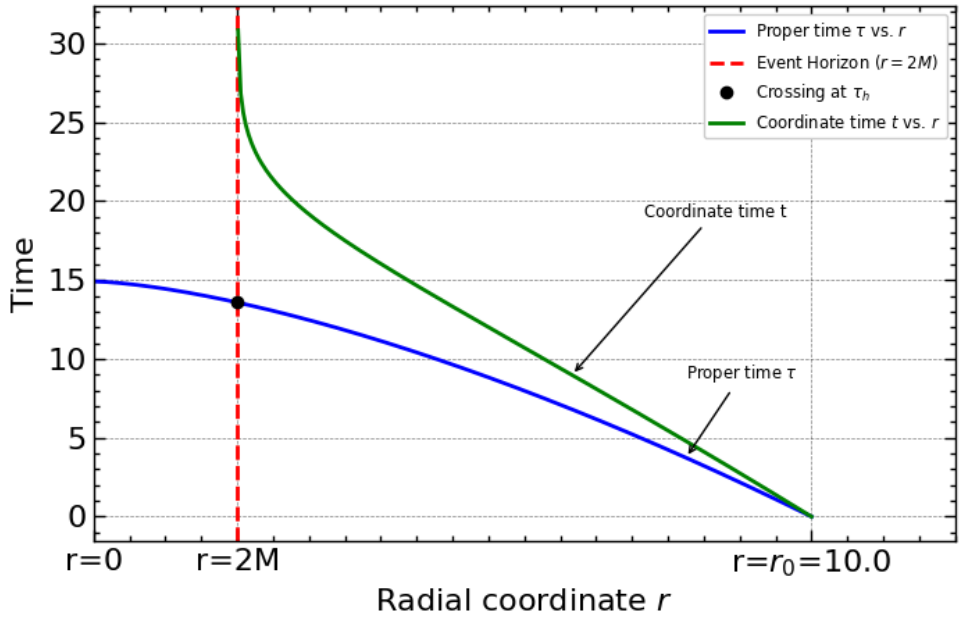

Figure 2. Radial infall of a test particle (dropped from rest at infinity) into a Schwarzschild black hole with M = 1 in spacetime coordinate convention. The blue curve shows the radial coordinate r versus the particle's proper time τ, while the green curve shows r versus the Schwarzschild coordinate time t. The vertical dashed line marks the event horizon at r = 2M, and the black dot indicates the horizon-crossing in proper time.

Equation 36 can be solved using numerical integration. We can visualize the motion of a radially infalling free particle in Schwarzschild spacetime by plotting both the coordinate time t and the proper time τ as functions of the radial coordinate r, thereby illustrating the distinct time evolutions experienced by a distant observer versus the particle itself.

3.1. *What happens to particles falling into Schwarzschild Black Hole? Is it the same for all Black Holes?*

As we saw, there are two natural ways to measure time for a falling particle. In the case of measuring proper time, we can see that a particle dropped from rest at infinity reaches the event horizon (r = 2M) in a finite proper time and continues to approach the physical singularity that is r = 0. This can be confirmed by the plot in figure 2. If we measure the coordinate time, t, we see that as the particle approaches the event horizon, i.e. r $\rightarrow$ 2M, the relation 36 dt/dr $\rightarrow \infty$. Thus, to an external observer, the particle appears to slow down and freeze, never quite reaching the event horizon in finite t. We can investigate this effect for other black hole solutions as well.

Reissner-Nordstrøm (Charged Black Hole) Solution: Reissner-Nordstrøm solution is for a charged black mass point. The line element for this solution is given as (J. Nordebo 2016):

$$ds^2 = \left(1 - \frac{2M}{r} + \frac{Q^2}{r^2}\right) dt^2 - \left(1 - \frac{2M}{r} + \frac{Q^2}{r^2}\right)^{-1} dr^2 - r^2(d\theta^2 + sin^2 d\phi^2) \tag{37}$$

When Q = 0, this reduces to the Schwarzschild solution. Compared to Schwarzschild (where the effective gravitational potential is proportional to $\frac{2M}{r}$) the charged solution includes an additional term $\frac{Q^2}{r}$. This term makes the gravitational attraction "shallower" at small r is Q is non-zero. If we take the metric function:

$$g_{00} = -{g_{00}}^{-1} = 1 - \frac{2M}{r} + \frac{Q^2}{r^2} \tag{38}$$

we can find the event horizon by taking $g_{00} = 0$, which gives us

$$r^2 - 2Mr + Q^2 = 1$$

. If we take $Q^2 > M^2$, the equation above has no real roots and is positive for all values of r which would be unphysical by cosmic censorship conjecture (R. M. Wald 1997). Then the metric in this case can be divided into three regions (J. Nordebo 2016):

1. Region 1: $r_+ < r < \infty$
2. Region 2: $r_- < r < r_+$
3. Region 3: $0 < r < r_-$

The more interesting case occurs when $Q^2 \leq M^2$, for then the metric has singularities when Q vanishes, namely at r = r_+ and r = r_-, where

$$r_\pm = M \pm \sqrt{M^2 - Q^2} \tag{39}$$

where r_+ is the outer horizon i.e. event horizon seen by distant observer and r_- is the inner horizon, also known as Cauchy horizon (G. Dotti 2019).

A freely falling particle starting from rest at infinity follows a geodesic for which one can derive an equation for the radial velocity:

$$\dot{r} = -\sqrt{\frac{2M}{r} - \frac{Q^2}{r^2}} \tag{40}$$

where the negative sign indicates inward motion. Despite the modifications due to charge, the integral of dτ remain finite as r approaches r_+, therefore, the particle would cross r_+ in finite proper time.

Kerr (Rotating Black Hole) Solution: The Kerr metric describes the rotating black hole solution. In Boyer-Lindquist coordinates, the line element is (S. A. Teukolsky 2015)

$$\begin{aligned} ds^2 = &\left(1 - \frac{2Mr}{\Sigma}\right) dt^2 - \frac{\Sigma}{\Delta} dr^2 - \Sigma\, d\theta^2 \\ &- \left(r^2 + a^2 + \frac{2Ma^2 r \sin^2\theta}{\Sigma}\right) \sin^2\theta\, d\phi^2 + \frac{4Mar\sin^2\theta}{\Sigma}\, dt\, d\phi, \end{aligned} \tag{41}$$

with

$$\Sigma = r^2 + a^2\cos^2\theta, \quad \Delta = r^2 - 2Mr + a^2, \quad a = \frac{J}{M}. \tag{42}$$

Frame Dragging:
The off-diagonal term in the Kerr metric (the $dt\, d\phi$ term) indicates that spacetime is dragged by the black hole's rotation. This *frame-dragging* effect forces all objects within a certain region to co-rotate with the black hole. In the Kerr metric, this effect is manifest in the term (G. V. Kraniotis 2005)

$$\frac{4Mar\sin^2\theta}{\Sigma}\, dt\, d\phi, \tag{43}$$

where

$$\Sigma = r^2 + a^2\cos^2\theta.$$

This term couples the time coordinate t and the angular coordinate ϕ, ensuring that even a particle dropped with zero angular momentum will acquire rotational motion.

Ergosphere:
Outside the event horizon lies the ergosphere, a region where no observer can remain static relative to infinity (S. A. Teukolsky 2015). The boundary of the ergosphere is determined by the surface where the time component of the metric, g_{tt}, changes sign. For the Kerr metric, we have

$$g_{tt} = 1 - \frac{2Mr}{\Sigma}. \tag{44}$$

The ergosurface is defined by the condition

$$1 - \frac{2Mr}{\Sigma} = 0. \tag{45}$$

Inside this region, the frame-dragging is so strong that all observers must co-rotate with the black hole.

Horizons:
The Kerr metric yields two horizons provided that $a < M$. These horizons are given by

$$r_\pm = M \pm \sqrt{M^2 - a^2}. \tag{46}$$

The outer horizon, r_+, functions as the event horizon. As in the Reissner–Nordström case, an infalling particle reaches r_+ in finite proper time, even though an external observer never sees the crossing due to coordinate time divergence.

The equation of motion for a particle falling radially in the equatorial plane ($\theta = \pi/2$) is more complicated in the Kerr geometry due to rotation. However, in a simplified model—often assuming the particle has zero angular momentum at infinity—the effective radial equation can be approximated by

$$\frac{dr}{d\tau} \approx -\sqrt{\frac{2Mr}{r^2 + a^2}}, \tag{47}$$

where τ is the proper time. This equation shows that the proper time experienced by the particle remains finite as it approaches and crosses the outer horizon.

The coordinate time t in Boyer–Lindquist coordinates is related to the proper time in a more intricate manner because of frame dragging and the non-spherical geometry. An approximate relation is given by

$$\frac{dt}{d\tau} \approx \frac{r^2 + a^2 + \frac{2Ma^2}{r}}{r^2 - 2Mr + a^2}. \tag{48}$$

Note that the denominator here is

$$\Delta = r^2 - 2Mr + a^2, \tag{49}$$

which vanishes at the outer horizon r_+. Hence, as $r \to r_+$,

$$\frac{dt}{d\tau} \to \infty,$$

implying that the coordinate time diverges at the horizon. For an external observer, the particle appears to slow down indefinitely and never cross the horizon in finite coordinate time.

Angular Motion:
Even if a particle is dropped radially (i.e. with zero initial angular momentum), the frame-dragging effect induces angular motion. The coupling between t and ϕ in the metric forces the particle to acquire an angular velocity. Although the geodesics become more complex, the key qualitative feature remains: the particle's proper time remains finite as it crosses r_+, while the coordinate time observed from infinity diverges near the horizon (G. V. Kraniotis 2005).

4. ADVANCE OF THE PERIHELION OF MERCURY

We now look at the one-body problem in general relativity. The advance of Mercury's perihelion is a classic example of a long-standing problem in gravitational physics. Its study is particularly instructive because it demonstrates how perturbative techniques in classical Newtonian dynamics can account for the dominant contributions to Mercury's orbital precession—primarily due to the gravitational influences of other planets. Once these classical effects are isolated, the remaining, very small residual precession can be attributed to the relativistic corrections from the Sun's gravitational field, which general relativity explains with precision.

4.1. *Solution to Perihelion Advance*

We assume that the central massive body (in this case the Sun) produces a spherically symmetric gravitational field. The appropriate solution in general relativity is then the Schwarzschild solution. The simplest approach is to start with the Lagrangian for this system:

$$\mathcal{L} = \frac{1}{2}\left[\left(1 - \frac{r_s}{r}\right)c^2\dot{t}^2 - \left(1 - \frac{r_s}{r}\right)^{-1}\dot{r}^2 - r^2\dot{\theta}^2 - r^2\sin^2\theta\,\dot{\phi}^2\right] \tag{50}$$

wehre dot denotes differentiation with respect to proper time τ and $r_s = \frac{2GM}{c^2}$ the Schwarzschild radius. If we confine the motion to the equatorial plane, i.e. $\theta = \frac{\pi}{2}$, then the reduced Lagrangian is:

$$\mathcal{L} = \frac{1}{2}\left[\left(1 - \frac{r_s}{r}\right)c^2\dot{t}^2 - \left(1 - \frac{r_s}{r}\right)^{-1}\dot{r}^2 - r^2\dot{\phi}^2\right] \tag{51}$$

We next work out the Euler-Lagrange equations. The Euler-Lagrange equation is of the form:

$$\frac{\partial}{\partial\tau}\left[\frac{\partial\mathcal{L}}{\partial\dot{x}^\nu}\right] - \frac{\partial\mathcal{L}}{\partial x^\nu} = 0 \tag{52}$$

It turns out to be sufficient to restrict attention to the two simplest equations, which are given by taking $\nu = 0{,}3$ in equation 52. These would now be:

$$\frac{\partial}{\partial\tau}\left\{\frac{\partial\mathcal{L}}{\partial\dot{t}}\right\} - \frac{\partial\mathcal{L}}{\partial t} = 0 \tag{53}$$

$$\frac{\partial}{\partial\tau}\left\{\frac{\partial\mathcal{L}}{\partial\dot{\phi}}\right\} - \frac{\partial\mathcal{L}}{\partial\phi} = 0 \tag{54}$$

Solving equation 53 to find the equation of motion for t, we get

$$\frac{\partial \mathcal{L}}{\partial t} = 0, \frac{\partial \mathcal{L}}{\partial \dot{t}} = \left(1 - \frac{r_s}{r}\right) c^2 \dot{t} \tag{55}$$

$$\frac{\partial}{\partial \tau}\left\{\left(1 - \frac{r_s}{r}\right) c^2 \dot{t}\right\} = \left(1 - \frac{r_s}{r}\right) c^2 \ddot{t} \tag{56}$$

Integrating equation 56 with respect to τ, we get

$$\int c^2 \left(1 - \frac{r_s}{r}\ddot{t}\right) d\tau = c^2 \left(1 - \frac{r_s}{r}\right) \dot{t} = k \tag{57}$$

where k is the constant of integration. Similarly, we solve equation 54 to find the equation of motion for ϕ

$$\frac{\partial \mathcal{L}}{\partial \dot{\phi}} = -r^2 \dot{\phi}, \frac{\partial}{\partial \tau}\left\{-r^2 \dot{\phi}\right\} = -r^2 \ddot{\phi}, \frac{\partial \mathcal{L}}{\partial \phi} = 0 \tag{58}$$

Therefore, the equation of motion for ϕ is

$$-r^2 \ddot{\phi} = 0 \tag{59}$$

Similar to equation 56, integrating equation 59 with respect to τ, we get

$$r^2 \dot{\phi} = h \tag{60}$$

where again h is the constant of integration. This equation shows the conservation of angular momentum, where h is the magnitude of the angular momentum per unit mass.

Since we can take the line element as $ds^2 = c^2 d\tau^2$, we know, the metric becomes

$$\left(1 - \frac{r_s}{r}\right) c^2 \dot{t}^2 - \left(1 - \frac{r_s}{r}\right)^{-1} \dot{r}^2 - r^2 \dot{\phi}^2 = c^2. \tag{61}$$

Let's introduce a new variable u = r^-1 and rearranging k so that $\dot{t} = \frac{k}{c^2}\left(1 - \frac{r_s}{r}\right)^{-1}$. Differentiating r with respect to ϕ we get

$$\frac{dr}{d\phi} = -\frac{1}{u^2}\frac{du}{d\phi} \tag{62}$$

Since

$$\dot{r} = \frac{dr}{d\tau} \Rightarrow \frac{\partial r}{\partial \phi}\frac{d\phi}{d\tau} \Rightarrow \frac{\partial r}{\partial \phi}\dot{\phi} \tag{63}$$

Therefore, substituting equation 62 in equation 64, we get

$$\dot{r} = -h\frac{du}{d\phi} \tag{64}$$

Then the differentiated elements in the metric become

$$\begin{aligned} \dot{\phi}^2 &= \frac{h^2}{r^4} = u^4 h^2 \\ \dot{t}^2 &= \frac{k^2}{c^4}\left(1 - \frac{r_s}{r}\right)^{-2} \end{aligned} \tag{65}$$

Therefore, the metric then becomes

$$\frac{k^2}{c^2} - \dot{r}^2 - u^2 h^2 \left(1 - \frac{r_s}{r}\right) = c^2 \left(1 - \frac{r_s}{r}\right) \tag{66}$$

Rearranging equation 66 for $\dot{r}^2$ and substituting the Schwarzschild radius and the value for $\dot{r}$ from equation 64, we get

$$h^2 \left(\frac{du}{d\phi}\right)^2 = \frac{k^2}{c^2} - u^2 h^2 + u^3 h^2 \frac{2GM}{c^2} - c^2 + c^2 u \frac{2GM}{c^2} \tag{67}$$

Rearranging equation 67, we get

$$\left(\frac{du}{d\phi}\right)^2 + u^2 = \frac{k^2 - c^2}{h^2 c^2} + \frac{2GM}{h^2}u + \frac{2GM}{c^2}u^3 \tag{68}$$

This is a first order differential equation for determining the orbit of a test particle, or more precisely the trajectory of the test body (in this case Mercury). Taking derivative of equation 68 with respect to ϕ, we get

$$2\frac{du}{d\phi}\frac{d^2u}{d\phi^2} + 2u\frac{du}{d\phi} = 0 + \frac{2GM}{h^2}\frac{du}{d\phi} + \frac{2GM}{c^2}\frac{du}{d\phi}3u^2 \tag{69}$$

Dividing both sides of the equation above by $2\frac{du}{d\phi}$ and substituting the value for u, we get

$$\frac{2}{r^3}\left(\frac{dr}{d\phi}\right)^2 - \frac{1}{r^2}\frac{d^2r}{d\phi^2} + \frac{1}{r} = \frac{GM}{h^2} + \frac{3GM}{c^2r^2} \tag{70}$$

This is the second order differential equation, and a relativistic version of the Binet's equation.

Visualising the Perihelion Orbits

In our investigation of the perihelion precession effect, we begin with the baseline parameters

$$\{G = 1,\ M = 1,\ c = 8,\ h = 1\},$$

which yield the standard orbit shown in figure 3a obtained from the Schwarzschild solution. The conservation laws derived from the Lagrangian lead to

$$\left(1 - \frac{r_s}{r}\right)c^2\dot{t} = k \quad \text{and} \quad r^2\dot{\phi} = h,$$

where $r_s = \frac{2GM}{c^2}$. With these default values, the relativistic correction causes a small perihelion advance, so that the orbit does not close exactly after an angular interval of 2π but rather after approximately which we will see later

$$2\pi\,(1 + \varepsilon) \quad \text{with} \quad \varepsilon \approx \frac{3GM^2}{h^2}.$$

In plot 3b, we reduce the speed of light to $c = 5$. Since the relativistic correction scales as $1/c^2$, a lower value of c amplifies the effect of spacetime curvature, resulting in a noticeably larger perihelion shift per orbit. Conversely, in plot 3c, we set $c = 20$, which diminishes the relativistic corrections and makes the orbit closer to the Newtonian closed ellipse, with a much smaller precession.

The plot 3d examines the impact of the angular momentum parameter by setting $h = 0.5$ (with M and c held constant). A reduction in h corresponds to a tighter orbit where the test particle comes closer to the Sun. This increases the gravitational field experienced at perihelion, thereby enhancing the relativistic precession effect.

By comparing these plots, one clearly sees that lower c, higher M, or lower h all lead to a more pronounced perihelion advance.

4.2. *Uniqueness of Perihelion Precession in Mercury's Orbit*

In Newtonian gravity the orbit of a test particle in a central potential is governed by the differential equation

$$\frac{d^2u}{d\phi^2} + u = \frac{GM}{h^2},$$

where $u = \frac{1}{r}$ and h is the specific angular momentum. Its general solution,

$$u(\phi) = \frac{GM}{h^2}\left[1 + e\cos\phi\right],$$

is exactly periodic with period 2π. In general relativity, however, an additional term appears in the orbital equation due to the curvature of spacetime, leading to

$$\frac{d^2u}{d\phi^2} + u = \frac{GM}{h^2} + 3GM\,u^2.$$

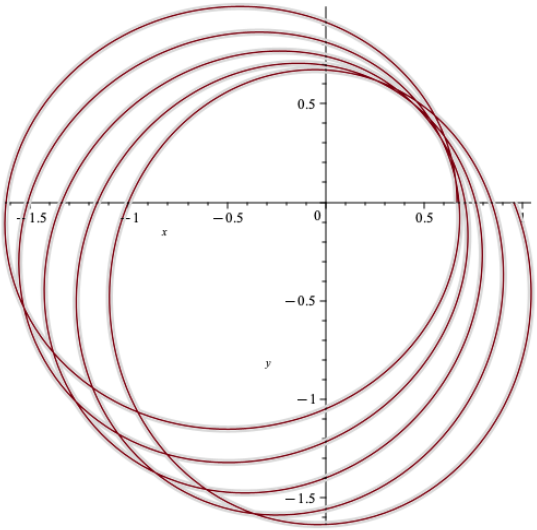

(a) Baseline orbit ($G = 1$, $M = 1$, $c = 8$, $h = 1$).

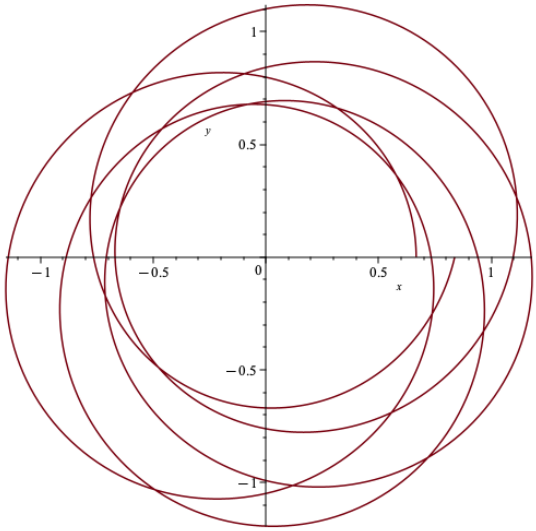

(b) Reduced speed of light ($c = 5$).

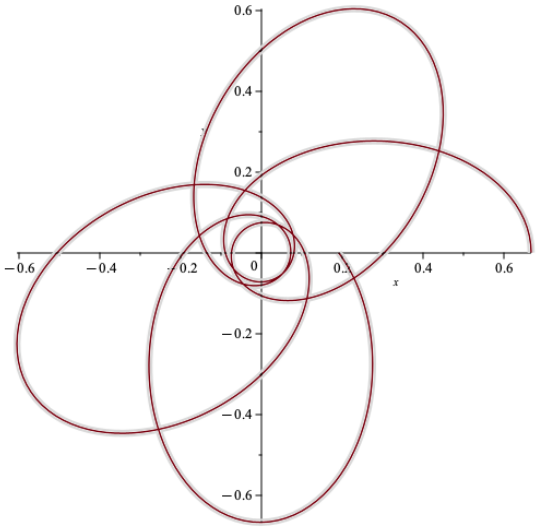

(c) Increased mass ($M = 5$ with $c = 20$).

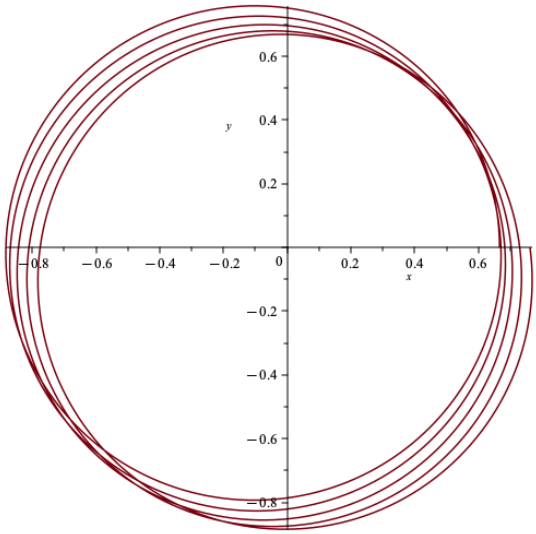

(d) Reduced angular momentum ($h = 0.5$ with $M = 5$ and $c = 20$).

Figure 3. Orbital plots showing the effect of parameter variations on the perihelion precession. Adjusting the speed of light, central mass, and angular momentum modifies the amount of perihelion advance observed.

This extra term perturbs the orbit so that the solution is more accurately represented by

$$u(\phi) = \frac{GM}{h^2}\left[1 + e\cos\big((1-\delta)\phi\big)\right],$$

where δ is a small positive parameter that quantifies the deviation from the Newtonian case. A perturbative analysis shows that

$$\delta \approx \frac{3GM}{c^2 a(1-e^2)},$$

where a is the semi-major axis and e is the eccentricity. Since the Newtonian relation for the specific angular momentum is

$$h^2 = GM\, a(1-e^2),$$

we can rewrite δ as

$$\delta \approx \frac{3GM^2}{c^2\, h^2}.$$

In a unit system where $c = 1$ (or after rescaling), we denote this small correction by ε, so that

$$\varepsilon = \frac{3GM^2}{h^2}.$$

Thus, the angle required for the orbit to close becomes approximately

$$2\pi(1 + \varepsilon),$$

rather than exactly 2π. This extra angle per orbit is the relativistic perihelion precession. Although all orbits in general relativity exhibit a small advance of the perihelion, Mercury's orbit is particularly affected because its close proximity to the Sun means that the gravitational field is much stronger there, resulting in a measurable precession.

5. EXTENDING THE PARTICLE TRAJECTORIES AND PERIHELION PRECESSION PHYSICS TO OTHER SPACETIMES

General relativity predicts that test particles follow geodesics determined by the spacetime metric. Two classic problems in this context are:

1. The **free-fall trajectory** of a particle into a black hole.
2. The **advance of the perihelion** in the orbit of a test body (in this case, Mercury).

Both phenomena are originally derived in the Schwarzschild spacetime. However, the same underlying methods can be extended to different spacetimes, such as the Reissner–Nordström (charged) and Kerr (rotating) solutions.

5.1. *Reissner–Nordström Spacetime for infalling particle*

The Reissner–Nordström metric for a charged black hole is (J. Nordebo 2016)

$$ds^2 = \left(1 - \frac{2M}{r} + \frac{Q^2}{r^2}\right) dt^2 - \left(1 - \frac{2M}{r} + \frac{Q^2}{r^2}\right)^{-1} dr^2 - r^2 \left(d\theta^2 + \sin^2\theta\, d\phi^2\right). \tag{71}$$

The geodesic equations are modified by the presence of the Q^2/r^2 term. A similar derivation yields

$$\dot{r} = -\sqrt{\frac{2M}{r} - \frac{Q^2}{r^2}}, \tag{72}$$

so that a particle falling from rest still reaches the outer horizon (located at $r_+ = M + \sqrt{M^2 - Q^2}$) in finite proper time, even though the coordinate time diverges as $r \to r_+$.

5.2. *Kerr Spacetime for infalling particle*

The Kerr metric for a rotating black hole in Boyer–Lindquist coordinates is (S. A. Teukolsky 2015)

$$\begin{aligned} ds^2 = &\left(1 - \frac{2Mr}{\Sigma}\right) dt^2 - \frac{\Sigma}{\Delta} dr^2 - \Sigma\, d\theta^2 \\ &- \left(r^2 + a^2 + \frac{2Ma^2 r \sin^2\theta}{\Sigma}\right) \sin^2\theta\, d\phi^2 + \frac{4Mar\sin^2\theta}{\Sigma}\, dt\, d\phi, \end{aligned} \tag{73}$$

with

$$\Sigma = r^2 + a^2\cos^2\theta, \quad \Delta = r^2 - 2Mr + a^2, \quad a = \frac{J}{M}. \tag{74}$$

In the equatorial plane ($\theta = \pi/2$), the metric simplifies, but the off-diagonal $dt\, d\phi$ term remains, representing frame dragging. Even if a particle is dropped radially with zero initial angular momentum, the rotation forces it to acquire angular motion (S. A. Teukolsky 2015; G. V. Kraniotis 2005). Nonetheless, one can derive an effective radial equation for the free-fall trajectory that shows the particle crosses the outer horizon (at $r_+ = M + \sqrt{M^2 - a^2}$) in finite proper time, while the coordinate time (defined in Boyer–Lindquist coordinates) diverges at the horizon.

5.3. *Reissner–Nordström Spacetime for Mercury's Perihelion Precession*

In the Reissner–Nordström metric, the additional term $\frac{Q^2}{r^2}$ modifies the effective potential. When one repeats the derivation of the orbital equation (with $u = 1/r$), extra terms appear which depend on Q. The general form becomes

$$\frac{d^2u}{d\phi^2} + u = \frac{GM}{h^2} + (\text{relativistic corrections}) + (\text{charge-dependent terms}). \tag{75}$$

These extra terms alter the magnitude of the perihelion advance, so that while a precession remains, its value depends on both M and Q (S. W. Hawking & G. F. R. Ellis 1973).

5.4. *Kerr Spacetime for Mercury's Perihelion Precession*

For the Kerr metric, in the equatorial plane the orbital dynamics are affected by the black hole's rotation through frame dragging. The effective orbital equation in the Kerr case includes the usual Schwarzschild-like correction plus additional terms involving the spin parameter a. Schematically, the equation becomes

$$\frac{d^2u}{d\phi^2} + u = \frac{GM}{h^2} + 3\frac{GM}{c^2}u^2 + (\text{terms involving } a). \tag{76}$$

Thus, the total perihelion advance in Kerr spacetime can be expressed as

$$\epsilon_{\text{Kerr}} \approx \frac{3GM^2}{c^2h^2} + \Delta_a, \tag{77}$$

where Δ_a represents additional contributions due to rotation (R. M. Wald 1984). Moreover, the frame-dragging effect may also induce precession of the orbital plane (Lense–Thirring precession).

5.5. *Limitations of These Extensions*

- **Test Particle Approximation:** The derivations assume that the orbiting body is of negligible mass.
- **Perturbative Methods:** The relativistic corrections are treated as small perturbations to the Newtonian orbit, an assumption that is valid in weak fields (e.g., Mercury's orbit) but may break down in stronger fields.
- **Symmetry Requirements:** These methods rely on the underlying spacetime being stationary and highly symmetric. In less symmetric or dynamic spacetimes, more advanced techniques (such as numerical relativity) are needed.
- **Coordinate Dependence:** Although the physical precession is coordinate-independent, the derivations are typically performed in specific coordinate systems (e.g., Schwarzschild or Boyer–Lindquist), which may obscure the global causal structure.

6. **CONCLUSION:**

In conclusion, the analysis of the Schwarzschild solution not only elucidates the structure of the gravitational field around a static, spherically symmetric mass, but also provides a fundamental framework for exploring more complex relativistic phenomena. For example, the study of free-fall trajectories reveals that a particle falling into a Schwarzschild black hole crosses the event horizon in a finite proper time, even though an external observer would measure an infinite coordinate time—a discrepancy that is illustrated by the Penrose diagram of the maximally extended spacetime. Likewise, when the orbital equation is reformulated in terms of $u = 1/r$, the inclusion of an extra relativistic term accounts for the observed advance of Mercury's perihelion. Extensions of this analysis to other spacetimes, such as the Reissner–Nordström and Kerr metrics, demonstrate that the finite proper-time infall and perihelion precession are preserved, the quantitative details are modified by additional influences, such as electric charge and rotation. These generalizations are subject to limitations, including the test-particle approximation, the reliance on perturbative methods applicable only in weak gravitational fields, and the idealized symmetry assumptions that may not hold in more dynamic or complex scenarios.

REFERENCES

2pt

Bergmann, P. G. 1962, The General Theory of Relativity, ed. S. Flügge (Berlin, Heidelberg: Springer Berlin Heidelberg), 203–272, doi: 10.1007/978-3-642-45973-3_3

Carroll, S. M. 1997, https://arxiv.org/abs/gr-qc/9712019

Carroll, S. M. 2019, Spacetime and Geometry: An Introduction to General Relativity (Cambridge University Press)

D'Inverno, R. 1992, Introducing Einstein's Relativity (Clarendon Press)

Dotti, G. 2019,, https://www.cosmo-ufes.org/uploads/1/3/7/0/13701821/dotti-vq19-2.pdf

Friedman, J. L., & Stergioulas, N. 2013, Lie derivatives, forms, densities, and integration, Cambridge Monographs on Mathematical Physics (Cambridge University Press), 349–368

Hawking, S. W., & Ellis, G. F. R. 1973, The Large Scale Structure of Space-Time (Cambridge University Press)

Horizon, B. T. 2024,, https://medium.com/@prmj2187/geometry-of-infinity-and-the-structure-of-space-time-8a2abc890234

Koiran, P. 2021, International Journal of Modern Physics D, 30, doi: 10.1142/s0218271821501066

Kraniotis, G. V. 2005, Classical and Quantum Gravity, 22, 4391–4424, doi: 10.1088/0264-9381/22/21/001

Lemos, J. P., & Silva, D. L. 2021, Annals of Physics, 430, 168497, doi: 10.1016/j.aop.2021.168497

MacCallum, M. A. 2013, Scholarpedia, 8, 8584, doi: 10.4249/scholarpedia.8584

Nordebo, J. 2016,, https://www.diva-portal.org/smash/get/diva2:912393/FULLTEXT01.pdf

Petersen, P. 2011,, https://www.math.ucla.edu/~petersen/Bianchi_Ricci_Identities.pdf

SCIAMA, D. W., WAYLEN, P. C., & GILMAN, R. C. 1969, Phys. Rev., 187, 1762, doi: 10.1103/PhysRev.187.1762

Shaikh, A. A., Ali, M., Salman, M., & Zengin, F. Ö. 2023, International Journal of Geometric Methods in Modern Physics, 20, 2350088

Sherwood, B. A. 2011. https://api.semanticscholar.org/CorpusID:18661248

Teukolsky, S. A. 2015, Classical and Quantum Gravity, 32, 124006, doi: 10.1088/0264-9381/32/12/124006

The Center for Cosmology and Particle Physics. 2018,, https://cosmo.nyu.edu/yacine/teaching/lectures

Tong, D. 2019,, https://www.damtp.cam.ac.uk/user/tong/gr/gr.pdf

Van Oosterhout, W. 2019,, https://annegretburtscher.wordpress.com/wp-content/uploads/2019/11/willemvanoosterhout_bscthesis_2019.pdf

Wald, R. M. 1984, General Relativity (University of Chicago Press)

Wald, R. M. 1997, https://arxiv.org/abs/gr-qc/9710068

Weyl, H. 2010–2011,, https://www.roma1.infn.it/teongrav/VALERIA/TEACHING/RELATIVITA_GENERALE/AA2010_11/simmetrie.pdf